Available online at www.sciencedirect.com
SCIENCE DIRECT®
International Journal of Heat and Mass Transfer 49 (2006) 3004–3015
International Journal of HEAT and MASS TRANSFER
www.elsevier.com/locate/ijhmt

Heat transfer in the thermal entrance region for flow through rectangular porous passages

A. Haji-Sheikh [a,*], D.A. Nield [b], K. Hooman [c]

[a] Department of Mechanical and Aerospace Engineering, The University of Texas at Arlington, 500 West First Street, Arlington, TX 76019-0023, USA
[b] Department of Engineering Science, University of Auckland, Private Bag 92019, Auckland, New Zealand
[c] Department of Mechanical Engineering, The University of Queensland, QLD 4072, Australia

Received 26 October 2005; received in revised form 4 January 2006
Available online 18 April 2006

Abstract

The study of heat transfer in rectangular passages with prescribed wall heat flux is of practical interest. These passages could be open or filled with saturated porous materials. A solution that uses the Green's function can accommodate the inclusion of heat flux over the entire surface area or over isolated sections of the boundary. Also, this solution permits the inclusion of frictional heating. Two different boundary conditions are considered: constant wall temperature and constant wall heat flux. The computed heat transfer coefficients show that the thermally fully developed condition may not be attainable in practical applications for very narrow passages with prescribed wall heat flux.

Keywords: Duct flow; Porous media; Forced convection; Weighted residuals; Rectangular ducts

1. Introduction

The placement of porous materials in passages can enhance the transfer of heat to a flowing fluid. Porous passages with rectangular cross-sections are useful devices for cooling of engineering systems. There has been a current interest in utilization of porous passages for electronic cooling applications; see e.g. [1]. Other applications are referenced in the review by Lage and Narasimhan [2]. A current general survey is contained in Nield and Bejan [3]. The particular topic of thermally developing forced convection in porous media is surveyed by Nield and Kuznetsov [4]. Recent papers involving porous-media forced convection in ducts of various shapes include those by Haji-Sheikh and Vafai [5] and Hooman and coworkers [6–8].

The computation of heat transfer rate in rectangular passages is the subject of this study. The temperature field in these passages may have different boundary conditions depending on the thermal conductivity of their impermeable enclosures. In this study, consideration is given to two different limiting boundary conditions that often appear in the literature: Constant uniform wall temperature and locally constant uniform wall heat flux. The first condition is appropriate when the thermal conductivity of the enclosing walls is sufficiently high. The prescribed local wall heat flux is the next limiting condition and it emerges when the uniformly heated walls of a passage are thin with relatively low conductivity. These two cases exhibit distinctly different and interesting features, especially in the thermally developing region. The analysis reveals that the coalescence of the thermal boundary layers from the opposite walls strongly depends on the distance between these walls if they are uniformly heated at a constant rate. For narrow rectangular passages, this phenomenon increases the length of the thermally developing region and makes the thermally fully developed condition unattainable in practical applications.

* Corresponding author. Tel.: +1 817 272 2010; fax: +1 817 272 2952.
E-mail address: haji@mae.uta.edu (A. Haji-Sheikh).

0017-9310/$ - see front matter © 2006 Elsevier Ltd. All rights reserved.
doi:10.1016/j.ijheatmasstransfer.2006.01.040

Nomenclature

A	area (m^2)
A	matrix
a	duct dimension, see Fig. 1
a_{ij}	elements of matrix **A**
B	matrix with elements b_{ij}
B_m	coefficients
b	duct dimension, see Fig. 1
b_{ij}	elements of matrix **B**
C	duct contour (m)
c_p	constant pressure specific heat (J/kg K)
D	matrix with elements d_{mj}
Da	Darcy number, K/a^2
D_h	hydraulic diameter $4A/C$ (m)
d_{mj}	elements of matrix **D**
E	matrix with elements e_{ij}
e_{ij}	elements of matrix **E**
$F_n(z)$	function, see Eq. (5)
f_i, f_j	basis functions
G	Green's function
h	heat transfer coefficient (W/m^2 K)
$\bar{h}$	average heat transfer coefficient (W/m^2 K)
i, j	indices
K	permeability (m^2)
k_e	effective thermal conductivity
M	μ_e/μ
m, n	indices
N	matrix dimension
Nu_D	Nusselt number, hD_h/k_e
$\overline{Nu}_D$	Nusselt number, $\bar{h}D_h/k_e$
P	matrix having elements p_{mi}
Pe	Peclet number, $\rho c_p a U/k_e$
Pr	Prandtl number, $\mu c_p/k_e$
p	pressure, Pa
p_{mi}	elements of matrix **P**
Re_D	Reynolds number, $\rho U D_h/\mu_e$
S	volumetric heat source (W/m^3)
T	temperature (K)
T_i	temperature at $x = 0$ (K)
U	average velocity (m/s)
$\overline{U}$	average value of $\bar{u}$
u	velocity (m/s)
$\bar{u}$	$\bar{u} = \mu u/(-a^2 \partial p/\partial x)$
x	axial coordinate (m)
$\hat{x}$	$(x/a)/Pe$
y, z	coordinates (m)
$\bar{y}, \bar{z}$	y/a and z/a

Greek symbols

β_m	eigenvalue
γ_m	eigenvalue
θ	dimensionless temperature
λ_m	eigenvalue
μ	fluid viscosity (N s/m^2)
μ_e	effective viscosity (N s/m^2)
ξ	dimensionless coordinate
ρ	fluid density (kg/m^3)
Φ	transformed temperature, Eq. (24)
ψ	eigenfunction

Subscripts

b	bulk
f	fluid
i	inlet condition
s	source effect
w	wall

The mathematical formulation of temperature for both cases of constant wall temperature and uniform wall heat flux is a necessary part of this presentation. The general solution to each of these two cases has a relatively large number of controlling parameters. Therefore, for brevity of this presentation, the effect of axial conduction is neglected.

2. Mathematical formulations

The basic working relations are the momentum and the energy equations. An exact solution for momentum equation provides the velocity field under a fully developed flow condition and it is available in [9]. The extended weighted residual method, described in [10], is employed in order to determine the temperature distribution from the energy equation. For completeness of this presentation, a brief description of the working relations is to follow.

2.1. Momentum equation

The working relations for the computation of velocity field are widely available in the literature. Their appearance in this paper is for the convenience of identification of the parameters in subsequent numerical analysis. For a laminar flow passing through rectangular passages, Fig. 1(a), with sufficiently high porosity, the entrance length is relatively small [11] and the flow is considered to be hydrodynamically fully developed. Accordingly, the Brinkman momentum equation, as used in Nield et al. [12–14] and Kuznetsov et al. [15] describes the velocity field; that is,

$$\mu_e\left(\frac{\partial^2 u}{\partial y^2}+\frac{\partial^2 u}{\partial z^2}\right)-\frac{\mu}{K}u-\frac{\partial p}{\partial x}=0 \tag{1}$$

wherein μ_e is the effective viscosity, μ is the fluid viscosity, K the permeability, and the pressure gradient $\partial p/\partial x$ is a constant. By setting $\bar{y} = y/a$, $\bar{z} = z/a$, $M = \mu_e/\mu$, and

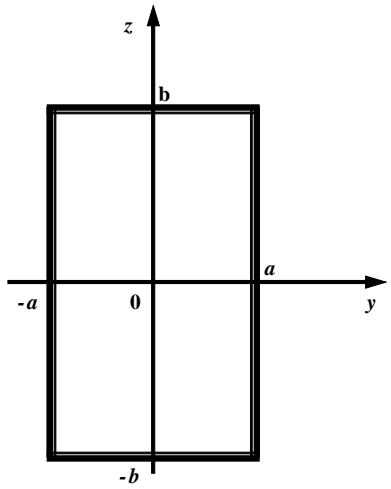

Fig. 1. A schematic of coordinates and dimensions of a rectangular passage.

$\bar{u} = \mu u/(-a^2\partial p/\partial x)$, Eq. (1) in the dimensionless form becomes

$$M\left(\frac{\partial^2 \bar{u}}{\partial \bar{y}^2} + \frac{\partial^2 \bar{u}}{\partial \bar{z}^2}\right) - \frac{1}{Da}\bar{u} + 1 = 0 \tag{2}$$

wherein $Da = K/a^2$ is the Darcy number and a is the characteristic length, see Fig. 1. The solution of Eq. (2), requires the condition of $\bar{u} = 0$ at the wall. Once the local velocity u is known, the mean velocity is

$$U = \frac{1}{A}\int_A u\,\mathrm{d}A \tag{3}$$

and then $\overline{U} = \mu U/(-a^2\partial p/\partial x)$.

A rapidly converging series solution of Eq. (2), is

$$\bar{u} = \frac{4}{\pi M}\sum_{n=1}^{\infty} F_n(\bar{z})\cos\frac{(2n-1)\pi\bar{y}}{2} \tag{4}$$

where

$$F_n(\bar{z}) = \frac{(-1)^{n-1}}{(2n-1)\beta_n^2}\left[1 - \frac{\cosh(\beta_n\bar{z})}{\cosh(\beta_n\bar{b})}\right] \tag{5}$$

and

$$\beta_n = \left[\frac{1}{MDa} + \frac{(2n-1)^2\pi^2}{4}\right]^{1/2} \tag{6}$$

The dimensionless mean velocity $\overline{U}$, using Eq. (3), is

$$\overline{U} = \frac{8}{\pi^2 M}\sum_{n=1}^{\infty}\frac{\beta_n\bar{b} - \tanh(\beta_n\bar{b})}{(2n-1)^2\bar{b}\beta_n^3} \tag{7}$$

and the normalized velocity is

$$\hat{u} = \frac{u}{U} = \frac{\bar{u}}{\overline{U}} = \frac{\pi}{2}\frac{\sum_{n=1}^{\infty}F_n(z)\cos[(2n-1)\pi y/2]}{\sum_{n=1}^{\infty}\frac{\beta_n\bar{b}-\tanh(\beta_n\bar{b})}{(2n-1)^2\bar{b}\beta_n^3}} \tag{8}$$

Also, a direct solution of Eq. (2) is a classical solution of the Poisson equation, and the normalized velocity, when $\beta_n = (n - 1/2)\pi$ and $\gamma_m = (m - 1/2)\pi/\bar{b}$, is

$$\hat{u} = \frac{u}{U} = \frac{\sum_{n=1}^{\infty}\sum_{m=1}^{\infty}\frac{4(-1)^{m+n}\cos(\beta_n\bar{y})\cos(\gamma_m\bar{z})}{\bar{b}\beta_n\gamma_m(\beta_n^2+\gamma_m^2+1/MDa)}}{\sum_{n=1}^{\infty}\sum_{m=1}^{\infty}\frac{4}{(\bar{b}\beta_n\gamma_m)^2(\beta_n^2+\gamma_m^2+1/MDa)}} \tag{9}$$

where $\bar{b} = b/a$. Using Eq. (9), it is possible to get an exact series solution for prescribed wall heat flux under the thermally fully developed condition. However, for numerical computations, Eq. (8) with single summation can provide an accurate solution at reduced computational time. As the preliminary step, the velocity field should be determined prior to its insertion into the energy equation. Eqs. (8) and (9), in addition to, a classical Galerkin solution of Eq. (2) were utilized as needed, the solution details are described in [10].

2.2. Governing energy equation

Under the local thermal equilibrium condition, the energy equation in its general form for hydrodynamically fully developed and incompressible flow is

$$(\rho c)_f u\frac{\partial T}{\partial x} = \frac{\partial}{\partial x}\left(k_e\frac{\partial T}{\partial x}\right) + \frac{\partial}{\partial y}\left(k_e\frac{\partial T}{\partial y}\right) + \frac{\partial}{\partial z}\left(k_e\frac{\partial T}{\partial z}\right) + S(x,y,z) \tag{10}$$

where $S(x,y,z)$ includes the contribution of frictional heating and parameters $(\rho c)_f$ and k_e are the fluid thermal capacity and the equivalent thermal conductivity, respectively. When the contribution of axial conduction is negligible, Eq. (10) reduces to

$$\frac{\partial}{\partial y}\left(k_e\frac{\partial T}{\partial y}\right) + \frac{\partial}{\partial z}\left(k_e\frac{\partial T}{\partial z}\right) + S(y,z;x) = (\rho c_p)_f u\frac{\partial T}{\partial x} \tag{11}$$

In the subsequent formulations ρc_p stands for $(\rho c_p)_f$. The solutions for Eq. (11) with a prescribed constant wall temperature and wall heat flux are the main objective of this study.

The next task is the computation of temperature in the entrance region of these rectangular passages. Because the velocity u depends on y and z while the functional form of temperature contains x in addition to y and z, the extended weighted residual method is a suitable solution technique. Assuming the thermophysical properties are independent of temperature and boundary conditions are homogeneous, the standard procedure [10,16] is to let

$$T(y,z;x) = \sum_{m=1}^{N} B_m\Psi_m(y,z)\mathrm{e}^{-\lambda_m^2 x} \tag{12}$$

where

$$\Psi_m = \sum_{j=1}^{N} d_{mj}f_j(y,z) \tag{13}$$

The eigenvalues are λ_m^2 and the coefficients d_{mj} are the members of eigenvectors $\mathbf{d}_m$; they are obtainable from the relation

$$(\mathbf{A} + \lambda_m^2\mathbf{B})\cdot\mathbf{d}_m = 0 \tag{14a}$$

where the elements of the matrices **A** and **B** are

$$a_{ij} = -\int_A k_e \nabla f_i(y,z)\cdot\nabla f_j(y,z)\,dA \tag{14b}$$

and

$$b_{ij} = \int_A \rho c_p u(y,z) f_i(y,z) f_j(y,z)\,dA \tag{14c}$$

The functions $f_i(y,z)$ and $f_j(y,z)$ are the basis functions and they must satisfy the appropriate homogeneous boundary conditions. After determination of λ_m^2 and d_{mj}, the appropriate mathematical steps in [10] provide the general solution. The eigenvectors $\mathbf{d}_m$ will constitute the rows of a matrix **D**. When the boundary conditions are homogeneous and the thermophysical properties are constant, the Green's function solution is

$$T(y,z;x) = \frac{1}{\rho c_p}\int_{\xi=0}^{x} d\xi \int_A GS(y',z';\xi)\,dA' + \int_A u(y',z')G(y,z,x|y',z',0)T(y',z';0)\,dA' \tag{15a}$$

wherein the Green's function G is

$$G(y,z,x|y',z',\xi) = \sum_{m=1}^{N}\left[\sum_{i=1}^{N} p_{mi} f_i(y',z')\right]\Psi_m(y,z)e^{-\lambda_m^2(x-\xi)} \tag{15b}$$

The parameters p_{mi} in Eq. (15b) are members of the matrix $\mathbf{P} = [(\mathbf{D}\cdot\mathbf{B})^{\mathrm{T}}]^{-1}$; details are in [16, Chapter 10]. Computer software is available to automatically determine the eigenvalues, eigenvectors, and matrix **P**; e.g., using the statements

(*amat = matix **A**, bmat = matrix **B**, dmat = matrix **D**, and pmat = matrix **P***)
abar = −Inverse[bmat].amat; eigv = Eigenvalues[abar];
dmat = Eigenvectors[abar];
pmat = Inverse[Transpose[dmat.bmat]];

in Mathematica [21]. Additionally, the general formulation of the Green's function in [16, Chapter 10] extends this solution to accommodate the nonhomogeneous boundary conditions.

The solution described by Eqs. (15a) and (15b) equally applies when using the boundary conditions of first, second, and even the third kind. The main difference is the selection of the basis functions f_j and these basis functions will be described in the subsequent computations for boundary conditions of the first kind and second kind.

2.2.1. Constant wall temperature solution

For this special case, the thermophysical properties have constant values and the governing energy equation (11) in dimensionless space, when $\hat{x} = (x/a)/Pe$, $\bar{y} = y/a$, $\bar{z} = z/a$, and $\theta = (T - T_w)/(T_i - T_w)$, has the following form

$$\frac{\partial^2\theta}{\partial\bar{y}^2} + \frac{\partial^2\theta}{\partial\bar{z}^2} + \frac{\mu_e U^2}{k_e(T_i - T_w)}\left[\frac{\hat{u}^2}{MDa} + \left(\frac{\partial\hat{u}}{\partial\bar{y}}\right)^2 + \left(\frac{\partial\hat{u}}{\partial\bar{z}}\right)^2\right] = \left(\frac{u}{U}\right)\frac{\partial\theta}{\partial\hat{x}} \tag{16}$$

The computational procedure for θ requires the selection of an appropriate set of basis functions that will satisfy the homogeneous boundary conditions of the first kind. Among many possible sets, the particular set

$$f_j = (1-\bar{y}^2)(\bar{b}^2 - \bar{z}^2)\bar{y}^{2(m_j-1)}\bar{z}^{2(n_j-1)}; \quad \text{for } j = 1,2,\ldots,N \tag{17}$$

is selected, using all combinations of $m_j = 1,2,\ldots$ and $n_j = 1,2,\ldots$ Next, the temperature solution was acquired using the aforementioned extended weighted residual method. First it is necessary to compute the members of matrices **A** and **B** by modifying Eqs. (14b) and (14c),

$$a_{ij} = -\int_{\bar{z}=0}^{\bar{b}}\int_{\bar{y}=0}^{1}\nabla f_i(\bar{y},\bar{z})\cdot\nabla f_j(\bar{y},\bar{z})\,d\bar{y}\,d\bar{z} \tag{18a}$$

and

$$b_{ij} = \int_{\bar{z}=0}^{\bar{b}}\int_{\bar{y}=0}^{1}\hat{u}(\bar{y},\bar{z}) f_i(\bar{y},\bar{z}) f_j(\bar{y},\bar{z})\,d\bar{y}\,d\bar{z} \tag{18b}$$

The temperature solution Eqs. (15a) and (15b) takes the following form

$$\theta(\bar{y},\bar{z};\hat{x}) = \frac{1}{\rho c_p}\int_{\hat{\xi}=0}^{\hat{x}} d\xi \int_{\bar{z}=0}^{\bar{b}}\int_{\bar{y}=0}^{1} G(\bar{y},\bar{z},\hat{x}|\bar{y}',\bar{z}',\xi)S(\bar{y}',\bar{z}')\,d\bar{y}'\,d\bar{z}' + \int_{\bar{z}=0}^{\bar{b}}\int_{\bar{y}=0}^{1} u(\bar{y}',\bar{z}')G(\bar{y},\bar{z},\hat{x}|\bar{y}',\bar{z}',0)\,d\bar{y}'\,d\bar{z}' \tag{19a}$$

wherein the Green's function is

$$G(\bar{y},\bar{z},\hat{x}|\bar{y}',\bar{z}',\xi) = \sum_{m=1}^{N}\left[\sum_{i=1}^{N} p_{mi} f_i(\bar{y}',\bar{z}')\right]\Psi_m(y,z)e^{-\lambda_m^2(\hat{x}-\xi)} \tag{19b}$$

and

$$S(\bar{y}',\bar{z}') = \frac{\mu_e U^2}{k_e(T_i - T_w)}\left[\frac{\hat{u}^2}{MDa} + \left(\frac{\partial\hat{u}}{\partial\bar{y}'}\right)^2 + \left(\frac{\partial\hat{u}}{\partial\bar{z}'}\right)^2\right] \tag{19c}$$

Once the temperature solution is known, the bulk temperature should be computed from the equation

$$\theta_b(\hat{x}) = \frac{1}{1\times\bar{b}}\int_{\bar{z}=0}^{\bar{b}}\int_{\bar{y}=0}^{1}\hat{u}(\bar{y},\bar{z})\theta(\bar{y},\bar{z};\hat{x})\,d\bar{y}\,d\bar{z} \tag{20a}$$

and then the Nusselt number, $Nu_D = hD_h/k_e$, is determined from the relation

$$Nu_D = -\frac{D_h^2}{4\theta_b}\frac{d\theta_b}{d\hat{x}} \tag{20b}$$

where $D_h = 4ab/(a+b)$ is the hydraulic diameter. In the absence of frictional heating, the frictional heating effect

vanishes, $S(\bar{y}',\bar{z}')=0$, and Eq. (19a) is then simplified accordingly.

Eqs. (17)–(20b) were utilized to compute the local and average Nusselt numbers. Fig. 2(a)–(d) are prepared to show the computed Nu_D for the four different aspect ratios $b/a=1,2,5,10$ as a function of $(x/a)/(Re_D Pr)$ where $Re_D=\rho U D_h/\mu_e$. Generally, the computation of energy input to a system is of interest in the design of heat transfer devices. In this application, the energy equation as applied to a volume element is

$$(a\times b)\rho c_p U\,\mathrm{d}T_b = q_w(a+b)\,\mathrm{d}x \tag{21a}$$

where q_w is the mean wall heat flux and $q_w=h(T_w-T_b)$. The substitution $h(T_w-T_b)$ for q_w in Eq. (21a) leads to the following relation

$$\left(\frac{ab}{a+b}\right)\rho c_p U\frac{\mathrm{d}T_b}{T_b-T_w}=-h\,\mathrm{d}x \tag{21b}$$

whose integration provides the local bulk temperature if the quantity

$$\bar{h}=\frac{1}{x}\int_0^x h\,\mathrm{d}x \tag{22}$$

called the average heat transfer coefficient is known. Therefore, the value of $\bar{h}$ is of practical interest. The data in Fig. 3(a)–(d) demonstrate the results from the computation of $\overline{Nu}_D=\bar{h}D_h/k_e$. The values of the Nusselt number when $MDa=0$ are obtained analytically using the classical product solution; therefore, from the bulk temperature relation in dimensionless space,

$$\frac{T_b-T_w}{T_i-T_w}=\left(\frac{1}{\bar{b}}\right)\left[2\sum_{m=1}^{\infty}\frac{\exp(-\gamma_m^2\hat{x})}{\gamma_m^2}\right]\left[\frac{2}{\bar{b}}\sum_{m=1}^{\infty}\frac{\exp(-\beta_m^2\hat{x})}{\beta_m^2}\right] \tag{23}$$

where $\hat{x}=(x/a)/Pe$, $\gamma_m=(m-1/2)\pi$, and $\beta_m=(m-1/2)\pi/\bar{b}$. The remaining lines were computed using the extended weighted residual method. The computed data in Fig. 3(a)–(d) are also for $\bar{b}=b/a=1,2,5$ and 10.

A sample of numerical data plotted in Figs. 2(a)–(d) and 3(a)–(d) are in Table 1. The objective was to select a number of basis functions that would provide a small error when $\hat{x}=10^{-3}$. As an example, for $m_j=1,2,\ldots,12$ and $n_j=1,2,\ldots,12$ in Eq. (17), the number of basis functions is $N=78$ with Eq. (13). This is a sufficiently large value of N for the worst case scenario presented here, $b/a=10$ and $MDa=10^{-4}$. This produced the first eigenvalue $\lambda_1^2=2.45867$ and the last eigenvalue $\lambda_{78}^2=14,119.5$ that would yield $\exp(-\lambda_{78}^2\hat{x})=\exp(-14,119.5\times10^{-3})=7.4\times10^{-7}$ at $\hat{x}=10^{-3}$. When using $m_j=1,2,\ldots,10$ and $n_j=$

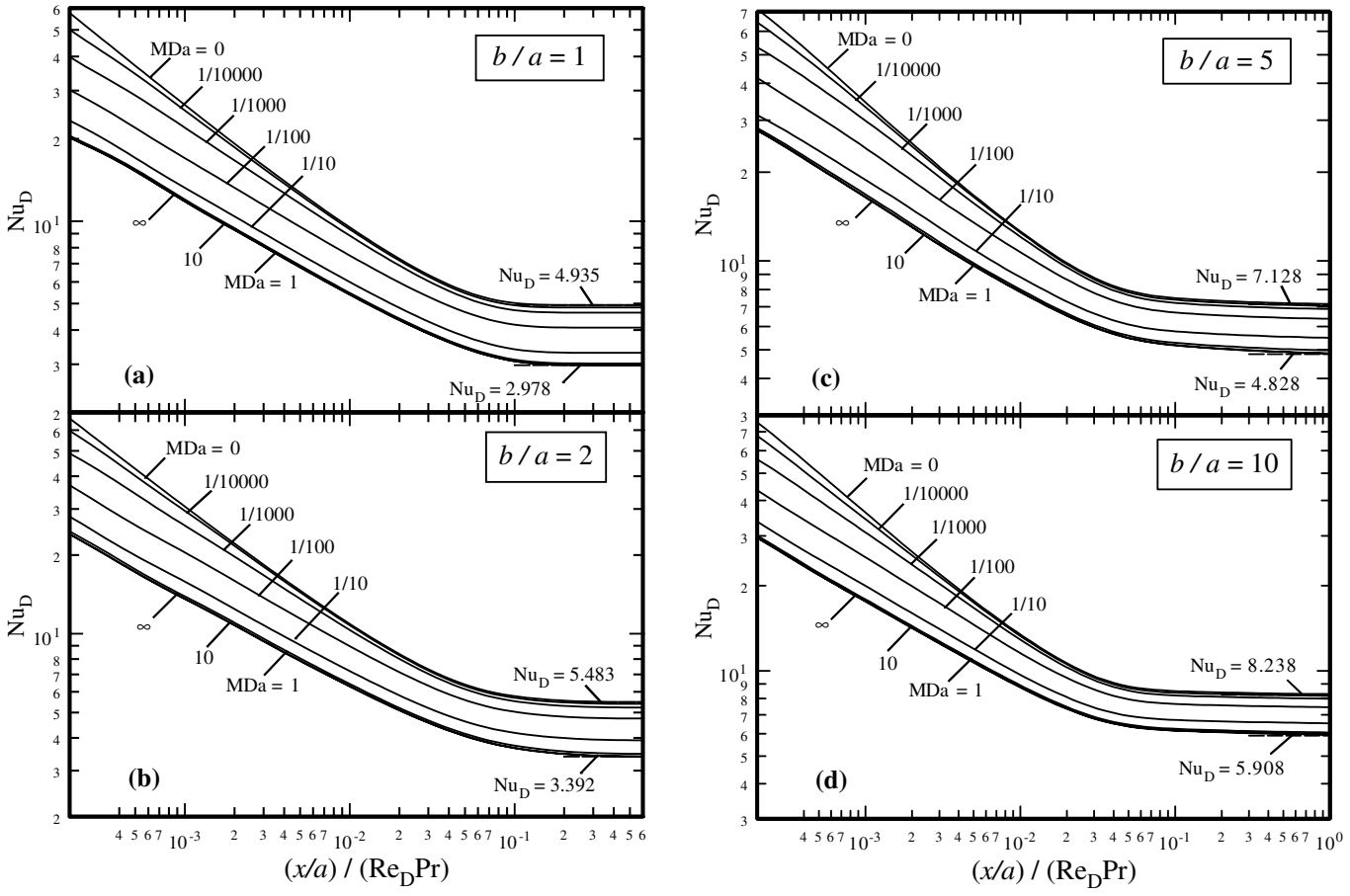

Fig. 2. Circumferentially averaged Nusselt number for rectangular passages with prescribed wall temperature when $b/a=1$ (a), 2 (b), 5 (c), and 10 (d).

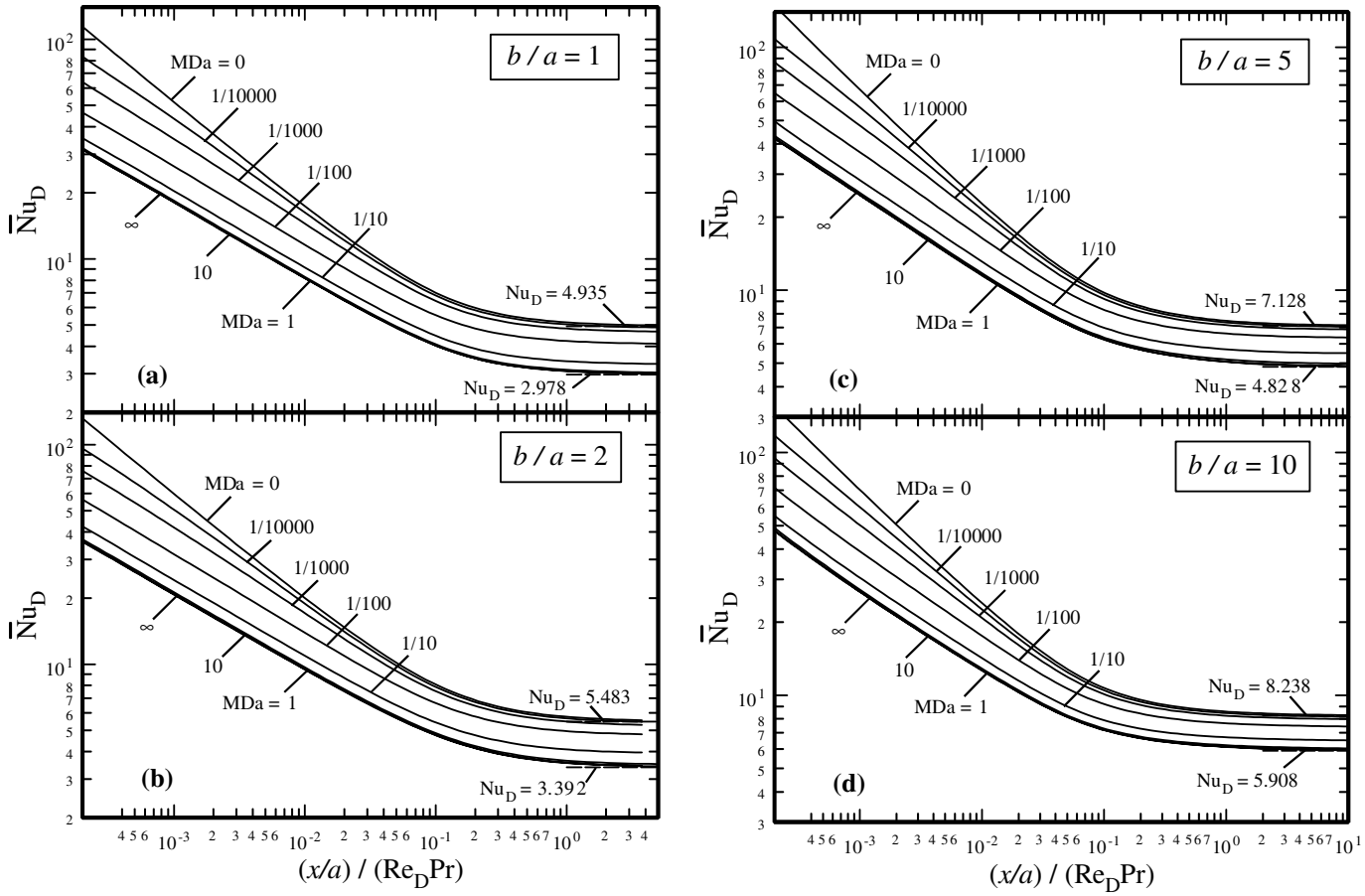

Fig. 3. Average Nusselt number for rectangular passages with prescribed wall temperature when $b/a = 1$ (a), 2 (b), 5 (c), and 10 (d).

$1, 2, \ldots, 10$ to reduce the number of basis functions to $N = 55$, the results show $\lambda_1^2 = 2.45467$ and a sufficiently large $\lambda_{55}^2 = 6525.26$. This indicates a reduced accuracy since $\exp(-\lambda_{55}^2 \hat{x}) = \exp(-6525.26 \times 10^{-3}) = 1.5 \times 10^{-3}$. Also, the first eigenvalues suffered a small change of 0.004 and that would directly influence the Nusselt number $Nu_D = (2/D_h)^2 \lambda_1^2$ under thermally fully developed condition. This deviation is mainly due to insufficient number of terms when computing the velocity profile and can be reduced by using Eq. (8) when MDa is very small. Therefore, as MDa increases, fewer basis functions are needed for sufficient accuracy. As an example, when using $b/a = 10$, $MDa = 10^{-2}$, and $N = 55$, the largest computed eigenvalues is $\lambda_{55}^2 = 18,685.3$ that should provide tabulated data with sufficient accuracy. Accordingly, when MDa is large, the error in the tabulated data is the truncation error. However, for smaller MDa parameter, the error is expected to remain within the last digit and it may get to the third digit when MDa is very small.

2.2.2. Locally constant wall heat flux solution

The next task is the computation of temperature in the entrance region of rectangular passages with locally constant wall heat flux q_w. As in the previous case, the thermophysical properties have constant values. One of the few methods to accommodate this boundary condition is to use a temperature transformation in the dimensionless form of the energy equation, Eq. (11),

$$\theta(\bar{y}, \bar{z}; \hat{x}) = \frac{T(y, z; x) - T_i}{q_w a / k_e} = \Phi(\bar{y}, \bar{z}; \hat{x}) + \frac{\bar{y}^2}{2} + \frac{\bar{z}^2}{2\bar{b}} \tag{24}$$

where $q_w = k_e \partial T/\partial y|_{y=a} = k_e \partial T/\partial z|_{z=b}$ is the input heat flux. After substituting for T from this transformation in Eq. (11), the function $\Phi(\bar{y}, \bar{z}; \hat{x})$ must satisfy equation

$$\frac{\partial^2 \Phi}{\partial \bar{y}^2} + \frac{\partial^2 \Phi}{\partial \bar{z}^2} + \frac{\mu_e U^2}{q_w a}\left[\frac{\hat{u}^2}{MDa} + \left(\frac{\partial \hat{u}}{\partial \bar{y}}\right)^2 + \left(\frac{\partial \hat{u}}{\partial \bar{z}}\right)^2\right] + \frac{\bar{b}+1}{\bar{b}} = \left(\frac{u}{U}\right)\frac{\partial \Phi}{\partial \hat{x}} \tag{25}$$

Moreover, the function $\theta(\bar{y}, \bar{z}; \hat{x})$ must satisfy the boundary conditions $\partial\Phi/\partial\bar{y}|_{\bar{y}=0} = \partial\Phi/\partial\bar{y}|_{\bar{y}=1} = 0, \partial\Phi/\partial\bar{z}|_{\bar{z}=0} = \partial\Phi/\partial\bar{z}|_{\bar{z}=\bar{b}} = 0$ and the entrance condition $\Phi(\bar{y}, \bar{z}; 0) = -(\bar{y}^2 + \bar{z}^2/\bar{b})/2$.

Eq. (25) contains a heat source expression that results from viscous dissipation in a porous medium modeled by the Brinkman equation, in the form recommended by Al-Hadhrami et al. [17]. An alternative expression was recommended by Nield [18]. For small values of Da the first term dominates over the remainder of the expression, and then

Table 1
A numerical sample of data appearing in Figs. 2(a)–(d) and 3(a)–(d)

MDa	$\hat{x}$	$b/a=1$		$b/a=2$		$b/a=5$		$b/a=10$	
		Nu_D	$\overline{Nu}_D$	Nu_D	$\overline{Nu}_D$	Nu_D	$\overline{Nu}_D$	Nu_D	$\overline{Nu}_D$
∞	0.001	15.08	22.76	18.92	28.88	24.43	36.74	26.37	7451
	0.01	6.730	10.28	8.606	13.09	11.34	17.05	12.76	763.9
	0.1	3.418	4.833	4.309	6.153	5.952	8.254	6.874	84.27
	1.0	2.978	3.193	3.405	3.806	4.973	5.448	6.040	14.01
	10	2.978	2.999	3.392	3.434	4.829	4.909	5.921	6.758
	∞	2.978	2.978	3.392	3.392	4.828	4.828	5.908	5.908
10	0.001	15.26	23.01	19.17	29.23	24.72	37.02	26.94	41.23
	0.01	6.790	10.37	8.691	13.22	11.82	17.73	12.90	19.14
	0.1	3.435	4.863	4.335	6.198	5.966	8.272	6.916	9.431
	1.0	2.982	3.200	3.414	3.820	4.986	5.461	6.053	6.494
	10	2.982	3.004	3.401	3.443	4.843	4.923	5.933	6.014
	∞	2.982	2.982	3.401	3.401	4.843	4.843	5.920	5.920
1	0.001	15.49	23.36	19.40	1262	25.25	37.83	27.40	42.11
	0.01	6.884	10.53	8.875	134.0	11.61	17.42	13.12	19.49
	0.1	3.477	4.927	4.418	18.64	6.065	8.423	7.006	9.574
	1.0	3.019	3.240	3.489	5.132	5.089	5.565	6.141	6.585
	10	3.019	3.041	3.476	3.642	4.953	5.032	6.028	6.107
	∞	3.019	3.019	3.476	3.642	4.953	4.953	6.016	6.016
10^{-1}	0.001	17.03	25.99	22.10	34.10	28.41	42.82	30.41	47.82
	0.01	7.568	11.62	9.990	15.30	12.91	19.59	14.50	21.71
	0.1	3.791	5.399	4.921	7.088	6.629	9.314	7.555	10.47
	1.0	3.303	3.544	3.930	4.376	5.591	6.103	6.610	7.098
	10	3.303	3.327	3.917	3.963	5.467	5.547	6.507	6.588
	∞	3.303	3.303	3.917	3.917	5.467	5.467	6.495	6.495
10^{-2}	0.001	21.94	33.77	28.97	45.06	36.46	56.19	38.92	63.18
	0.01	9.539	14.86	12.67	19.78	16.14	25.11	17.89	27.46
	0.1	4.653	6.731	5.963	8.827	7.790	11.36	8.754	12.61
	1.0	4.082	4.380	4.754	5.309	6.477	7.131	7.529	8.163
	10	4.082	4.112	4.743	4.800	6.348	6.442	7.418	7.515
	∞	4.082	4.082	4.743	4.743	6.348	6.348	7.406	7.406
10^{-3}	0.001	28.81	45.48	38.59	60.63	47.31	78.82	50.09	83.36
	0.01	11.59	18.97	15.28	25.17	19.25	31.55	21.03	34.10
	0.1	5.258	7.955	6.592	10.30	8.480	13.07	9.467	14.38
	1.0	4.632	4.997	5.236	5.898	6.989	7.779	8.065	8.834
	10	4.632	4.668	5.228	5.295	6.858	6.965	7.949	8.061
	∞	4.632	4.632	5.227	5.227	6.858	6.858	7.938	7.938
10^{-4}	0.001	34.53	57.74	45.71	75.42	55.26	92.09	59.57	102.7
	0.01	12.47	21.90	16.35	28.82	20.48	35.69	22.40	38.83
	0.1	5.458	8.522	6.778	10.96	8.677	13.81	9.680	15.20
	1.0	4.835	5.236	5.403	6.114	7.157	8.006	8.251	9.084
	10	4.835	4.875	5.396	5.468	7.026	7.139	8.133	8.251
	∞	4.835	4.835	5.396	5.396	6.996	6.996	8.122	8.122

the distinction between the two alternatives is a fine one. The two alternatives are treated by Nield et al. [19]. Some general aspects of viscous dissipation in the context of forced convection in a porous medium are discussed by Nield [20].

Neglecting the contribution of viscous dissipation, the quantity $(\bar{b}+1)/\bar{b}$ remains as the only contribution to $S(y',z',\xi)$ in the Green's function solution for $\Phi(\bar{y},\bar{z};\hat{x})$ when using Eqs. (15a) and (15b). As in the previous case, the velocity distribution is computed using the Galerkin method and a Fourier series solution for the purpose of verification of accuracies, especially, when b/a is large. As to the temperature solution, the following set of basis functions satisfy the homogeneous boundary condition of the second kind along the walls,

$$f_j = [1+(m_j-1)(1-\bar{y}^2)] \times [1+(n_j-1)(1-\bar{z}^2/\bar{b}^2)]\bar{y}^{2(m_j-1)}\bar{z}^{2(n_j-1)} \quad (26)$$

for all combinations of $m_j = 1,2,\ldots$ and $n_j = 1,2,\ldots$ This function is to be placed for f_j and then for f_i in Eqs. (18a) and (18b), after replacing j with i, to get the new members of the matrices **A** and **B**. As before, Eq. (14a) provides the eigenvalues and eigenvectors for the determination of $\mathbf{d}_m$

vectors located in the rows of the **D** matrix. Next, the relation $\mathbf{P}=[(\mathbf{D}\cdot\mathbf{B})^{\mathrm{T}}]^{-1}$ produces the members of matrix **P** for inclusion in the Green's function solution,

$$\theta(\bar{y},\bar{z};\hat{x}) = \left(\frac{\bar{y}^2}{2}+\frac{\bar{z}^2}{2\bar{b}}\right) + \int_{\xi=0}^{\hat{x}} \mathrm{d}\xi \int_{\bar{z}=0}^{\bar{b}} \int_{\bar{y}=0}^{1} G(\bar{y},\bar{z},\hat{x}|\bar{y}',\bar{z}',\xi) \times \left(\frac{1+\bar{b}}{\bar{b}}\right) \mathrm{d}\bar{y}'\,\mathrm{d}\bar{z}' - \int_{\bar{z}=0}^{\bar{b}} \int_{\bar{y}=0}^{1} u(\bar{y}',\bar{z}') G(\bar{y},\bar{z},\hat{x}|\bar{y}',\bar{z}',0) \times \left(\frac{\bar{y}^2}{2}+\frac{\bar{z}^2}{2\bar{b}}\right) \mathrm{d}\bar{y}'\,\mathrm{d}\bar{z}' \tag{27a}$$

where the Green's function

$$G(\bar{y},\bar{z},\hat{x}|\bar{y}',\bar{z}',\xi) = \sum_{m=1}^{N} \left[\sum_{i=1}^{N} p_{mi} f_i(\bar{y}',\bar{z}')\right] \Psi_m(\bar{y},\bar{z}) \mathrm{e}^{-\lambda_m^2(\hat{x}-\xi)} \tag{27b}$$

contains new sets of basis functions $f_i(\bar{y}',\bar{z}')$, eigenfunctions $\Psi_m(\bar{y},\bar{z})$, parameters p_{mi}, and eigenvalues λ_m^2.

Once the temperature solution $\theta(\bar{y},\bar{z};\hat{x})$ is available, the following equation provides the mean wall temperature,

$$\theta_{\mathrm{w}}(\hat{x}) = \frac{1}{1+\bar{b}} \left[\int_{\bar{y}=0}^{1} \theta(\bar{y},\bar{b};\hat{x})\,\mathrm{d}\bar{y} + \int_{\bar{z}=0}^{\bar{b}} \theta(1,\bar{z};\hat{x})\,\mathrm{d}\bar{z}\right] \tag{28}$$

Under the constant wall heat flux condition, the energy balance leads to a relation for the bulk temperature,

$$\frac{T_{\mathrm{b}}-T_{\mathrm{i}}}{q_{\mathrm{w}}a/k_{\mathrm{e}}} = \frac{1+\bar{b}}{\bar{b}}\hat{x} \tag{29}$$

It is also computed analytically from Eq. (20a), with $\theta(\bar{y},\bar{z};\hat{x})$ from Eq. (24), for the verification of the mathematical relations for the temperature solution. If one designates $\theta_{\mathrm{w}} = (T_{\mathrm{w}}-T_{\mathrm{i}})/(q_{\mathrm{w}}a/k_{\mathrm{e}})$ and $\theta_{\mathrm{b}} = (T_{\mathrm{b}}-T_{\mathrm{i}})/(q_{\mathrm{w}}a/k_{\mathrm{e}})$, the Nusselt number is obtainable from the relation $Nu = ha/k_{\mathrm{e}} = 1/(\theta_{\mathrm{w}}-\theta_{\mathrm{b}})$ and then using the hydraulic diameter $D_{\mathrm{h}} = 4ab/(a+b)$ in the definition, the Nusselt number becomes

$$Nu_{\mathrm{D}} = \frac{D_{\mathrm{h}}}{a}Nu = \frac{4\bar{b}}{1+\bar{b}}\left(\frac{1}{\theta_{\mathrm{w}}-\theta_{\mathrm{b}}}\right) \tag{30}$$

Fig. 4(a)–(d) show the Nusselt numbers computed for $b/a = 1$, 2, 5, and 10 and plotted versus $(x/D_{\mathrm{h}})/(Re_{\mathrm{D}}Pr)$ where $Re_{\mathrm{D}}Pr = D_{\mathrm{h}}\rho c_p U/k_{\mathrm{e}}$ and $D_{\mathrm{h}} = 4ab/(a+b)$. To illustrate the variations of the wall temperature, θ_{w} and θ_{b} are plotted in Fig. 5(a)–(d) for the same aspect ratios. A sample of numerical data appearing in these figures is also tabulated in Table 2. The data have similar convergence characteristics as discussed for those appearing in Table 1. However,

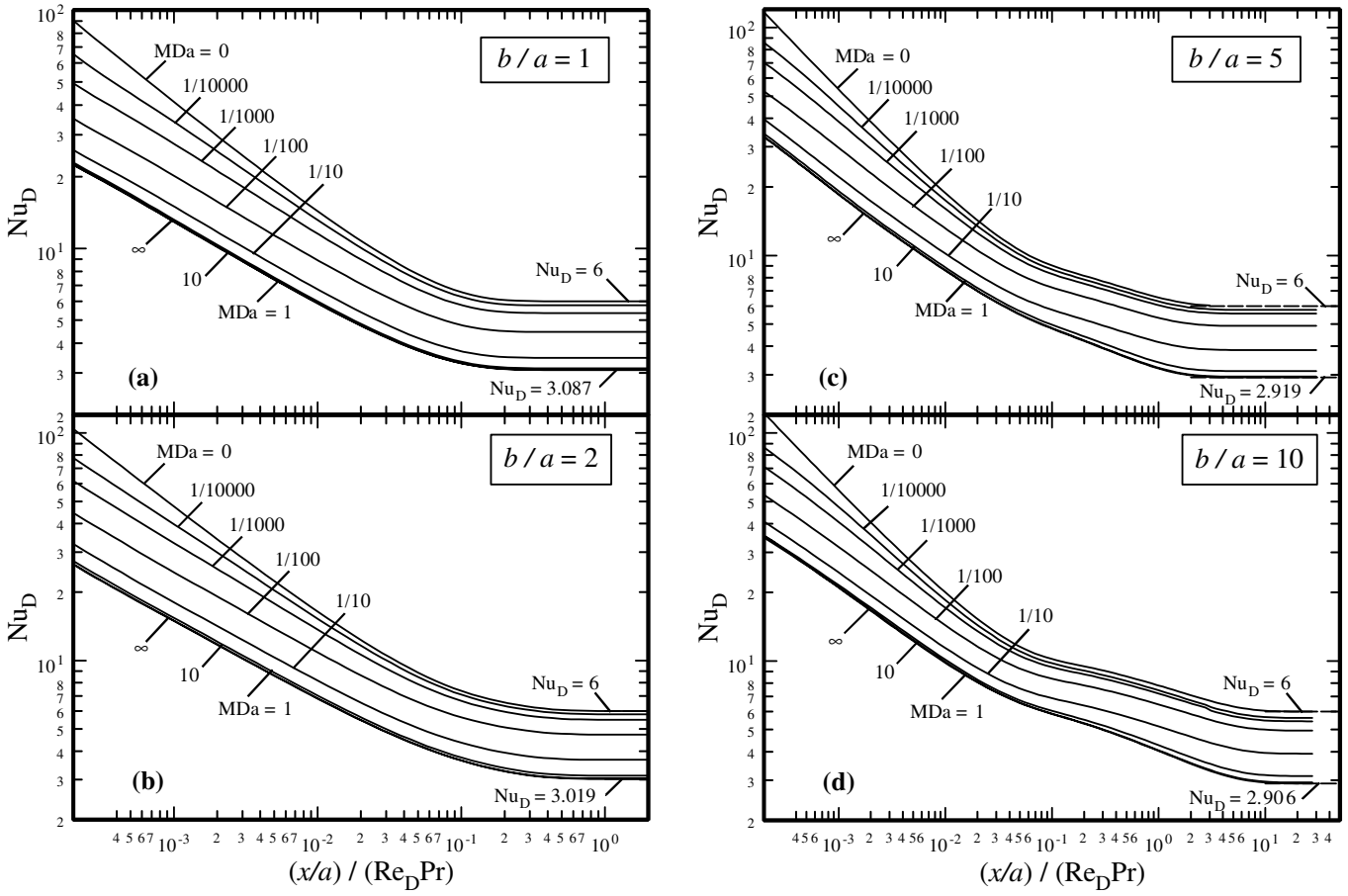

Fig. 4. Circumferentially average Nusselt number for rectangular passages with prescribed wall heat flux when $b/a = 1$ (a), 2 (b), 5 (c), and 10 (d).

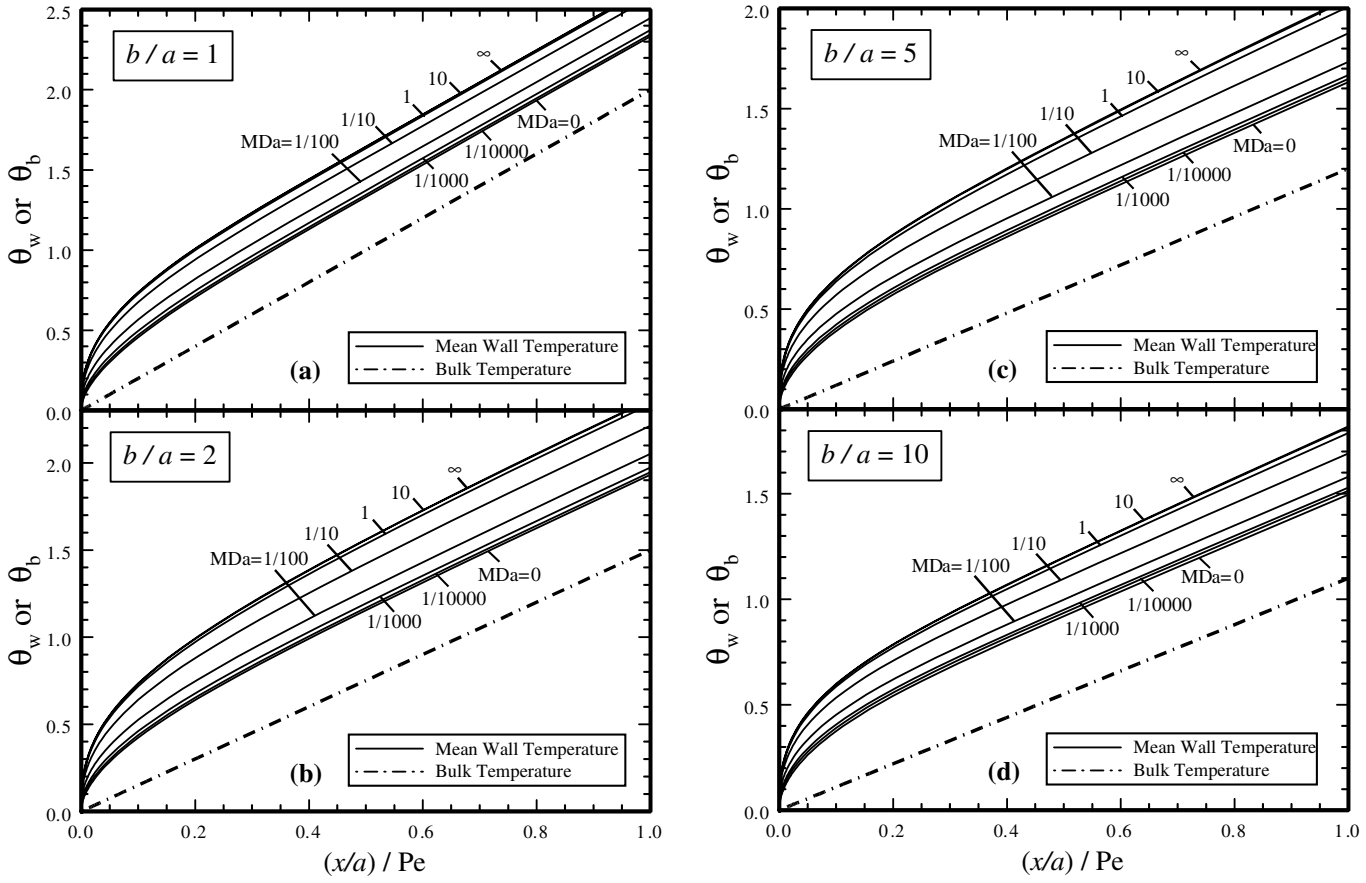

Fig. 5. Mean wall temperature of rectangular passages with prescribed wall heat flux when $b/a = 1$ (a), 2 (b), 5 (c), and 10 (d).

for this case, the thermally fully developed solution can be compared with the exact series solution [9].

3. Results and discussion

An examination of Nu_D data in Fig. 2(a)–(d) indicates that a thermally fully developed condition is attainable when $(x/a)/(Re_D Pr) \gtrsim 0.5$. Only small changes are detectable by examining individual figures in Fig. 2(a)–(d). The data in Table 1 clearly show this trend. The data show that 1% departure from the fully developed Nu_D value occurs at $(x/a)/(Re_D Pr) \approx 0.15$ when $b/a = 1$ for all MDa values. However, there is a small deviation when $b/a = 2$ as this 1% deviation occurs at $(x/a)/(Re_D Pr) \approx 0.21$ for slug flow when $MDa = 0$ and at $(x/a)/(Re_D Pr) \approx 0.27$ for open channel flow when $MDa = \infty$. This trend continues for other aspect ratios as this 1% departure from the fully developed condition is within $(x/a)/(Re_D Pr) \approx 0.49$–$0.71$ when $b/a = 5$ and it slightly changes from $(x/a)/(Re_D Pr) \approx 0.52$–$0.8$ when $b/a = 10$, for a range of MDa between 0 and ∞.

However, the situation changes significantly when the wall heat flux is prescribed. Fig. 4(a) shows that a thermally fully developed condition is also attainable when $(x/a)/(Re_D Pr) \approx 0.5$ while this limit increases as b/a increases and it exceeds 10 in Fig. 4(d). Moreover, this situation remains the same for all MDa values in Fig. 4(a)–(d). This unique and interesting feature, for the case of prescribed wall heat flux, deserves a more detailed study for a better understanding of this phenomenon. A sample of data for different b/a and MDa values, appearing in Table 2, indicate this trend.

It is appropriate to study the limiting condition when $MDa \to 0$ as this can provide useful information for all MDa values. In the absence of frictional heating, the exact solution of Eq. (25) with prescribed wall heat flux q_w is

$$\frac{T - T_i}{q_w a/k} = \theta(\bar{y}, \bar{z}; \hat{x}) = \frac{1}{2}\left[(\bar{y})^2 + \left(\bar{z}/\bar{b}\right)^2\right] + \hat{x}[1 + (1/\bar{b})^2] - \frac{1+\bar{b}}{6} - 2\sum_{n=0}^{\infty} \frac{(-1)^n}{n^2\pi^2} \cos(n\pi\bar{y}) \exp[-n^2\pi^2\hat{x}] - 2\bar{b}\sum_{n=0}^{\infty} \frac{(-1)^n}{n^2\pi^2} \cos(n\pi\bar{z}/\bar{b}) \exp[-n^2\pi^2\hat{x}/\bar{b}^2] \quad (31)$$

where, as before, $\bar{b} = b/a$ and $\hat{x} = (x/a)/Pe$ when $Pe = a\rho c_p U/k_e$. This equation can provide the temperature within the thermal entrance region with a high degree of accuracy when $\bar{b}$ is very large. The terms in these series exponentially reduce as n becomes large and this solution

Table 2
A numerical sample of data appearing in Figs. 4(a)–(d) and 5(a)–(d)

MDa	$\hat{x}$	$b/a = 1$		$b/a = 2$		$b/a = 5$		$b/a = 10$	
		Nu_D	θ_w	Nu_D	θ_w	Nu_D	θ_w	Nu_D	θ_w
∞	0.001	16.51	0.1231	20.99	0.1285	28.65	0.1175	32.08	0.1145
	0.01	7.399	0.2903	9.458	0.2969	12.66	0.2753	14.93	0.2546
	0.1	3.725	0.7369	4.562	0.7345	6.243	0.6539	7.447	0.5983
	1.0	3.087	2.648	3.081	2.366	3.915	2.051	5.059	1.819
	10	3.087	20.65	3.019	15.88	2.933	13.14	3.352	12.08
	∞	3.087	∞	3.019	∞	2.919	∞	2.9060	∞
10	0.001	16.55	0.1229	21.07	0.1280	28.77	0.1171	31.66	0.1160
	0.01	7.415	0.2897	9.492	0.2959	12.71	0.2743	15.06	0.2524
	0.1	3.732	0.7359	4.577	0.7326	6.267	0.6519	7.463	0.5973
	1.0	3.092	2.647	3.092	2.362	3.939	2.046	5.085	1.815
	10	3.092	20.65	3.030	15.88	2.955	13.13	3.380	12.08
	∞	3.092	∞	3.030	∞	2.941	∞	2.933	∞
1	0.001	16.88	0.1205	21.74	0.1242	29.65	0.1136	32.31	0.1136
	0.01	7.549	0.2849	9.770	0.2879	13.09	0.2668	15.43	0.2467
	0.1	3.788	0.7280	4.702	0.7171	6.451	0.6367	7.643	0.5858
	1.0	3.136	2.638	3.186	2.337	4.119	2.009	5.283	1.788
	10	3.136	20.64	3.123	15.85	3.127	13.07	3.592	12.01
	∞	3.136	∞	3.123	∞	3.112	∞	3.132	∞
10^{-1}	0.001	19.11	0.1067	25.71	0.1052	34.30	0.0984	37.04	0.0993
	0.01	8.518	0.2548	11.42	0.2486	15.11	0.2326	17.43	0.2196
	0.1	4.208	0.6753	5.444	0.6398	7.403	0.5703	8.592	0.5332
	1.0	3.472	2.576	3.737	2.214	4.933	1.876	6.152	1.691
	10	3.472	20.58	3.663	15.73	3.868	12.86	4.447	11.82
	∞	3.472	∞	3.663	∞	3.849	∞	3.929	∞
10^{-2}	0.001	25.74	0.0797	35.13	0.0774	45.79	0.0740	48.42	0.0762
	0.01	11.36	0.1961	15.33	0.1890	19.85	0.1799	22.32	0.1739
	0.1	5.467	0.5658	7.109	0.5251	9.374	0.4756	10.62	0.4524
	1.0	4.461	2.448	4.829	2.052	6.246	1.734	7.564	1.581
	10	4.461	20.45	4.726	15.56	4.941	12.67	5.602	11.65
	∞	4.461	∞	4.726	∞	4.915	∞	4.983	∞
10^{-3}	0.001	35.46	0.0584	48.10	0.0569	60.95	0.0559	64.18	0.0579
	0.01	14.96	0.1537	19.91	0.1489	25.17	0.1444	27.82	0.1419
	0.1	6.742	0.4966	8.593	0.4603	11.03	0.4221	12.28	0.4062
	1.0	5.351	2.374	5.628	1.974	7.118	1.669	8.463	1.530
	10	5.351	20.37	5.494	15.49	5.601	12.60	6.244	11.58
	∞	5.351	∞	5.494	∞	5.569	∞	5.608	∞
10^{-4}	0.001	44.73	0.0467	59.77	0.0461	73.95	0.0463	77.56	0.0480
	0.01	17.47	0.1345	22.97	0.1311	28.40	0.1294	31.29	0.1272
	0.1	7.389	0.4707	9.294	0.4369	11.73	0.4042	12.98	0.3901
	1.0	5.762	2.347	5.957	1.948	7.419	1.649	8.769	1.515
	10	5.762	20.35	5.808	15.46	5.813	12.57	6.429	11.57
	∞	5.762	∞	7.543	∞	5.779	∞	5.839	∞

can produce accurate data at small values of $\hat{x}$ by predetermining the number of needed term in this series. Next, using Eq. (31) for $\theta(\bar{y},\bar{z};\hat{x})$, as before, Eqs. (28) and (29) will determine the mean wall temperature $\theta_w = (T_w - T_i)/(q_w a/k_e)$ and the bulk temperature $\theta_b = (T_b - T_i)/(q_w a/k_e)$. Then, the Nusselt number is obtainable from the relation $Nu = ha/k_e = 1/(\theta_w - \theta_b)$ and, when using the hydraulic diameter in the definition, Eq. (30) yields the Nusselt number Nu_D.

For slug flow, $MDa = 0$, though rectangular ducts, Fig. 6 shows the unique behavior of this limiting Nusselt number for different values of $\bar{b} = b/a$ ratios. An inflection point, detectable in Fig. 4(c) and (d), is also detectable in Fig. 6. It shows that there is a change in the shape of these curves as b/a increases. This change is clearly visible for $b/a \geqslant 5$. As an example, when $b/a \geqslant 50$, the thermally fully developed condition exists when $(x/a)/Re_D Pr \approx 1000$. Also, this Fig. 6 shows that a thermally fully developed condition may not be attainable in practical applications and the parallel plate solution is a viable choice for very narrow channels.

The temperature variation at the wall, when b/a is large, also can assist in the understanding of this Nusselt number behavior. The data in these figures are indicative of a unique behavior in the entrance region of rectangular passages. It was noted that there is a significant change in the

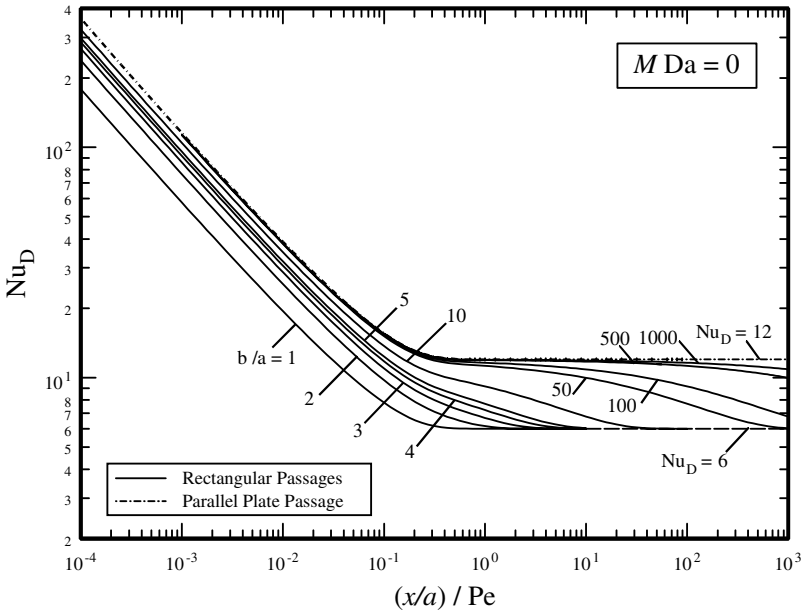

Fig. 6. Nusselt numbers for slug flow through rectangular passages with prescribed wall heat flux.

wall temperature of the rectangular passage as $\hat{x} = (x/a)/Pe$ increases beyond 10^{-2}; earlier, the temperature profile is nearly flat. Fig. 7(a) and (b) are prepared to illustrate the variation of $(\theta - \theta_b)$ as $\hat{x}$ increases. Fig. 7(a) is plotted when $y = a$ and the temperature $(\theta - \theta_b)$ changes as z/a changes along the wall. Similarly, Fig. 7(b) is plotted when $z = b$ and the temperature $(\theta - \theta_b)$ changes as y/a changes along the wall. It is a representative of the temperature behavior when MDa is very small. The solid lines are for $MDa = 0$ using exact analysis while the dot-dash lines are for $MDa = 10^{-4}$ using this extended weighted residual method.

We hypothesize that the axial locations of the inflexion points correspond to the coalescence of the thermal boundary layers, arising on opposite walls of the enclosure, that thicken as the fluid travels downstream. If the position of the first coalescence (involving the shorter dimension of the cross-section of the channel) and that of the second coalescence are x_1 and x_2, respectively, then scale analysis leads to the expectation that $x_1 = \varepsilon a^2 \rho c_p U/k_e$ and $x_2 = \varepsilon b^2 \rho c_p U/k_e$, where ε is a constant of order unity. According to the data in Fig. 4(a), $\varepsilon \approx 1/2$. This implies that $x_2/x_1 = (b/a)^2$ as the data in Fig. 6 would indicate. As an example, the thermally fully developed entrance condition for $b/a = 10$ extends to about 100 times larger than that for $b/a = 1$. As an illustration, assuming $a = 1$ cm when $b/a = 10$, the thermal entrance length is $x/a = 50 \times Pe$ and, when $Pe = 20$, it becomes $x = 1000 \times a$ or 10 m.

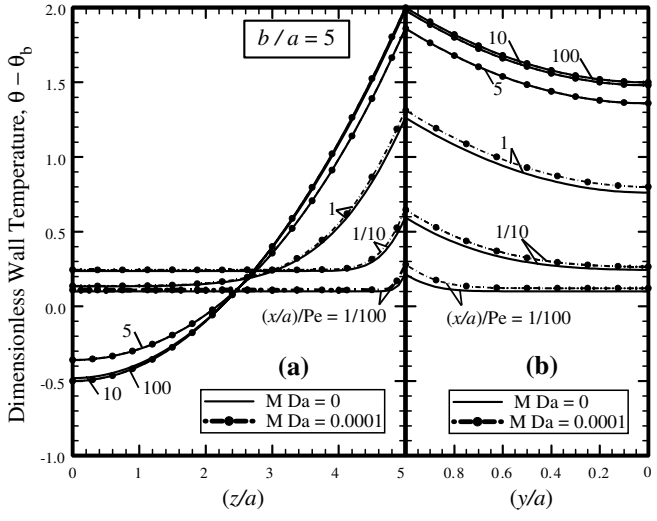

Fig. 7. Typical wall temperature variations of a rectangular passage under thermally fully developed condition and prescribed wall heat flux.

4. Conclusion

A Green's function solution based on the variational calculus is a viable method to study heat transfer in fluid flow passages. The rectangular duct serves as a mean of demonstrating the viability of this method for application to flow in porous passages. Also, the methodology presented in this paper equally applies when the velocity profile has other forms [22,23]. However, the inclusion of the contribution of axial conduction and/or local thermal non-equilibrium requires a significant undertaking. A change of basis function permits its extension to other geometries. Using symbolic algebra on modern software can produce results with high degree accuracy away from entrance location. At small values of axial coordinate, a larger number of basis functions are needed and an accurate solution can become demanding. However, this problem exists for other types of series solutions including the exact one.

The results indicate a unique and interesting behavior when a rectangular channel is heated uniformly at a constant rate from all sides. For these channels with large b/a, the thermal entrance length can increase by a factor of $\sim(b/a)^2$. This would indicate that a thermally fully developed condition may not be attainable in practical applications when aspect ratio is large.

References

[1] J.L. Lage, A.K. Weinert, D.C. Price, R.M. Weber, Numerical study of low permeability micorporous heat sink for coiling phased-array radar systems, Int. J. Heat Mass Transfer 39 (1996) 3622–3647.

[2] J.L. Lage, A. Narasimhan, Porous media enhanced forced convection fundamentals and applications, in: K. Vafai (Ed.), Handbook of Porous Media, Marcel Dekker, New York, 2000, pp. 357–394.

[3] D.A. Nield, A. Bejan, Convection in Porous Media, third ed., Springer-Verlag, New York, 2006.

[4] D.A. Nield, A.V. Kuznetsov, Forced convection in porous media: transverse heterogeneity effects and thermal development, in: K. Vafai (Ed.), Handbook of Porous Media, second ed., Taylor and Francis, New York, 2005, pp. 143–193.

[5] A. Haji-Sheikh, K. Vafai, Analysis of flow and heat transfer in porous media imbedded inside various-shaped ducts, Int. J. Heat Mass Transfer 47 (2004) 1889–1905.

[6] K. Hooman, Fully developed temperature distribution in porous saturated duct of elliptical cross-section, with viscous dissipation effects and entropy generation analysis, Heat Transfer Res. 36 (2005) 237–245.

[7] K. Hooman, H. Gurgenci, Effects of temperature-dependent viscosity variation on entropy generation, heat, and fluid flow through a porous-saturated duct of rectangular cross-section, Appl. Math. Mech. submitted for publication.

[8] K. Hooman, A.A. Merrikh, Analytical solution of forced convection in a duct of rectangular cross-section saturated by a porous medium, ASME J. Heat Transfer, in press.

[9] A. Haji-Sheikh, Fully developed heat transfer to fluid flow in rectangular passages filled with porous materials, ASME J. Heat Transfer 128 (6) (2006) 822–828.

[10] A. Haji-Sheikh, E.M. Sparrow, W.J. Minkowycz, Heat transfer to flow through porous passages using extended weighted residuals method—A Green's function solution, Int. J. Heat Mass Transfer 48 (2005) 1330–1349.

[11] K. Kaviany, Principles of Heat Transfer in Porous Media, Springer-Verlag, New York, 1991.

[12] D.A. Nield, A.V. Kuznetsov, M. Xiong, Thermally developing forced convection in a porous medium: parallel-plate channel or circular tube with walls at constant heat flux, J. Porous Med. 6 (2003) 203–212.

[13] D.A. Nield, A.V. Kuznetsov, M. Xiong, Thermally developing forced convection in a porous medium: parallel-plate channel or circular tube with isothermal walls, J. Porous Med. 7 (2004) 19–27.

[14] D.A. Nield, A.V. Kuznetsov, M. Xiong, Thermally developing forced convection in a porous medium: parallel plate channel with walls at uniform temperature, with axial conduction and viscous dissipation effects, Int. J. Heat Mass Transfer 46 (4) (2003) 643–651.

[15] A.V. Kuznetsov, M. Xiong, D.A. Nield, Thermally developing forced convection in a porous medium: circular ducts with walls at constant temperature, with longitudinal conduction and viscous dissipation effects, Transport Porous Med. 53 (3) (2003) 331–345.

[16] J.V. Beck, K. Cole, A. Haji-Sheikh, B. Litkouhi, Heat Conduction Using Green's Functions, Hemisphere Publ. Corp., Washington, DC, 1992.

[17] A.K. Al-Hadhrami, L. Elliot, D.B. Ingham, A new model for viscous dissipation in porous media across a range of permeability values, Transport Porous Med. 53 (2003) 117–122.

[18] D.A. Nield, Comments on 'A new model for viscous dissipation in porous media across a range of permeability values', Transport Porous Med. 55 (2004) 253–254.

[19] D.A. Nield, A.V. Kuznetsov, M. Xiong, Effects of viscous dissipation and flow work on forced convection in a channel filled by a saturated porous medium, Transport Porous Med. 56 (2004) 351–367.

[20] D.A. Nield, A note on a Brinkman–Brinkman forced convection problem, Transport Porous Med., in press.

[21] S. Wolfram, The Mathematica Book, fourth ed., Cambridge University Press, 1999.

[22] S.Y. Kim, J.-M. Koo, A.V. Kuznetsov, Effect of anisotropy in permeability and effective thermal conductivity on thermal performance of an aluminum foam heat sink, Numer Heat Transfer A 40 (1) (2001) 21–36.

[23] P.-X. Jiang, Z.-P. Ren, B.-X. Wang, Numerical simulation of forced convection in porous plate channels using thermal equilibrium and nonthermal equilibrium models, Numer. Heat Transfer A 35 (1999) 99–113.